Available online at www.sciencedirect.com
ScienceDirect
International Journal of Thermal Sciences 48 (2009) 936–947
International Journal of Thermal Sciences
www.elsevier.com/locate/ijts

Simulation on the thermal cycle of a welding process by space–time convection–diffusion finite element analysis

Shaodong Wang [a,*], John Goldak [a], Jianguo Zhou [b], Stanislav Tchernov [b], Dan Downey [b]

[a] *Carleton University, Ottawa, ON, K1S 5B6, Canada*
[b] *Goldak Technologies Inc., Ottawa, ON, K1V 7C2, Canada*

Received 6 February 2008; received in revised form 11 July 2008; accepted 16 July 2008

Available online 20 August 2008

Abstract

Welding plays an important role in manufacturing. But difficulties still exist for simulation of the welding process of large welded structures, due to the limitation of computer capacity, mathematical models and software. This paper is devoted to developing an algorithm that tries to simulate the thermal cycle during welding efficiently and accurately. A space–time finite element method (FEM) is proposed to solve the transient convection–diffusion thermal equation. The method has been applied to the steady-state thermal analysis of welds. A moving coordinate frame (Eulerian frame), in which the heat source is stationary, is used to improve the spatial resolution of a numerical analysis for the thermal cycle of welds effectively, as well as to incorporate the addition of the filler metal naturally. This method is suitable for the thermal analysis in the weld pool or/and weld joint region including starting and stopping transients.

Keywords: Welding; Thermal cycle; Convection–diffusion; Space–time; Finite element method; Eulerian

1. Introduction

The temperature field in the welding process is extremely inhomogeneous and transient. For material points inside the weld seam, temperatures can range from room temperature to above melting point. During the thermal cycle, filler metals and base metals which are inside the weld pool melt, solidify and recrystallize. Meanwhile, microstructural transformations take place in the heat-affected-zone (HAZ). Therefore, the temperature field determines the welding residual stress and distortion not only directly through the thermal strains, but also indirectly through the transformation strains that accompany the changes in the microstructure and the temperature dependence of material properties such as yield stress.

The early attempts to analyze the flow of heat in the welding process were by Rosenthal [1] and Rykalin [2], who independently developed analytic solutions, which were based on an Eulerian formulation, to solve the heat equation for moving heat sources. Their solutions then became the primary analytical method for computing the steady state temperature fields in welding [3]. However, there are limitations in these analytical solutions: (1) geometry and heat input models are simplified; (2) material property values are assumed to be temperature independent; and (3) heat transfer and heat radiation from the surface to the ambient environment are often simplified or even neglected.

Since the 1980s, with the advancement of the computer technology, the finite element method (FEM) has become popular for computing the transient temperature fields in welding. The transient Lagrangian formulation allowed the analysis of complex geometry as well as nonlinear equations. Many successful 2-dimensional and 3-dimensional transient analyses on welds have been developed [4–6]. To simulate the temperature field of a weldment by using a Lagrangian formulation, however, there are three major concerns [7]:

- To represent properly the sharp temperature gradient around the heat source, a very fine mesh inside and near the weld pool is required. Commonly, there are two methods to realize this: (1) a fine space discretization is implemented

* Corresponding author.
E-mail address: shaodong.wang@nrc-cnrc.gc.ca (S. Wang).

1290-0729/$ – see front matter
doi:10.1016/j.ijthermalsci.2008.07.007

Nomenclature

b	coefficient for heat loss
C	constant of value approximately 1
c_p	specific heat capacity
$\mathcal{E}$	reference spatial element
f_x	flux on Neumann boundary
h	local mesh size
H	enthalpy
I, I_n	time domain
J	spatial element Jacobian
$\mathbf{J}$	space–time element Jacobian
k	thermal conductivity
k_n	time interval length
$\mathbf{n}$	outward normal unit vector on surface
$\wp$	space–time physical element
q	heat transferred from heat source to plate
Q	heat source term
r	a measure of the residual
R	transitional electrical resistance
$\mathbf{R}$	vector of spatial basis functions
$\Re$	space–time reference element
R_0	modified Bessel function of second kind and zero order
S, S_n	space–time domain and slab
t, t_n	time in physical element
Δt	physical time interval length
T	temperature
$\mathbb{T}$	upper bound of time domain
T_f	final temperature
$\mathcal{T}$	reference element in time
$\mathbf{u}$	velocity vector
v	velocity of the moving heat source
$\mathbf{V}$	velocity field on the physical domain
W, W_n	space–time domain for discretization
x, y, z	Cartesian coordinates

Greek symbols

α	thermal diffusivity
α'	modified thermal diffusivity
Γ	boundary of the domain
δ	stabilizing factor
Δ	thickness of the plate
θ	test functions
λ_{ij}	space–time basis functions
λ_c	coefficient of convective heat transfer
λ_r	coefficient of heat radiation
ρ	density
τ^1, τ^3	time in reference element
$\Delta\tau$	reference time element interval length
φ_i	spatial basis functions
Φ	distribution function
χ^1, χ^3	basis functions on reference time element
Ω	space domain
ξ, η, ζ	coordinates in reference element

Subscripts and superscripts

0	initial condition
D	Dirichlet boundary condition
in	inflow boundary
N	Neumann boundary condition

along the whole weld path, or (2) the mesh is updated dynamically with a small mesh size inside and near the weld pool region while the heat source moves [8].

- To lessen or even avoid the numerical effect of "spot welding", a very small time step size is also required. This leads to a large number of time steps that can consume a huge amount of computing time and data storage space.
- To include the addition of the filler metal, the geometry or mesh must be updated while the weld pool moves, which can be complex and costly. Therefore, the addition of the filler metal has often been ignored in Lagrangian FEM formulations. However, solidification of the filler material will release a large amount of enthalpy, which may affect the temperature distribution in the region after the molten pool and in the HAZ. In fact, a correct temperature distribution history is critical for microstructure evolution and thermal stress analyses [9].

To address these difficulties, Gu [7] proposed a transformed FEM Eulerian formulation to compute the steady state temperature field in welds. It allowed a much higher spatial resolution than a transient Lagrangian formulation, and only needed one time step. Also, the addition of the filler metal becomes natural in an Eulerian formulation. However, like Rosenthal's solution, the resulting energy equation assumed constant thermal properties, which may raise questions.

Rajadhyaksha and Michaleris [10] proposed an Eulerian finite element formulation, to optimize a quasi-static thermal process using a SUPG formulation. They concluded that an Eulerian formulation can drastically reduce the computational run-time, and then can be applied to the optimization of quasi-state processes. Chen et al. [11] also reported the reduction of running time and data storage through the use of an Eulerian moving coordinate frame for the welding thermal analysis. Compared to the transient Lagrangian formulation, they found the Eulerian formulation to be more accurate and efficient.

In this paper, a nonlinear, transient FEM algorithm with temperature dependent material properties is presented that uses a space–time finite element formulation to solve the transient convection–diffusion thermal equation. The space–time finite element mesh uses basis functions that are continuous in space but discontinuous in time. It retains the advantages that an Eulerian frame possesses: high spatial resolution, large time step size without "spot welding" effect and filler metal added naturally. In fact, this space–time formulation allows the material velocity and mesh velocity to be varied independently. Thus, it

is capable of gracefully dealing with the full spectrum of the Arbitrary Lagrangian–Eulerian (ALE) methods ranging from a Lagrangian frame to an Eulerian frame. The Eulerian frame is a special case of the space–time formulation.

For a long weld with a constant welding velocity, a quasi-steady state solution of the thermal histories can be found over most of the middle part of the weld joint in the Eulerian frame if the frame fixed with the heat source. For a one-meter butt weld, the region of end-transients is about 15 cm on both ends [12]. So, for long welds, the quasi-steady state assumption for the middle part is reliable. It is also very practical because many real welds are often several meters in length. A steady state can be obtained by running a transient analysis until it approaches the steady state. Normally, this algorithm is suitable for the weld pool and weld joint region. It is expected that the nonlinear transient analysis in the Lagrangian frame would converge more rapidly if the solution of a quasi-steady state analysis is used as the first approximation.

Although a steady state Eulerian method [7,10,11] may be more effective for an infinitely long weld with constant cross-section, it cannot deal with the starting and ending transients of starting and stopping a weld. The proposed space–time method can deal gracefully and naturally with the starting and ending transients of starting and stopping a weld. Furthermore, the space–time method appears to have the potential to deal with the important cases of pulsed welds and welds with weaving.

2. Space–time finite element

To accommodate the addition of the filler metal and the moving weld pool during the welding processes, the finite element method is used in both the space and time dimensions.

For the space–time continuum domain, if space and time are treated equivalently, the idea of discretizing this continuum by use of space–time finite elements comes naturally. However, due to the fact that information is transferred only from earlier to later times, we do not need to have a global coupling of the variables in the time dimension, but still we wish to retain the standard step-wise approach from finite differences. To achieve this we use a continuous Galerkin method for discretization in space and a discontinuous method for discretization in time, by using an arbitrary polynomial order [13–18].

Let $0 = t_0 < t_1 < t_2 < t_3 < \cdots < t_{\mathbb{N}} = \mathbb{T}$ be a sequence of times and a partition of the time interval $[0, \mathbb{T}]$, and let $\Omega(t)$ be a space domain that can change from one time-step to another. A space–time "slab" S_n is defined as the set of all ordered pairs (x, y, z, t), with $(x, y, z) \in \Omega(t)$ and t in the interval $I_n = [t_n, t_{n+1}]$, of length $k_n = t_{n+1} - t_n$; if Ω has no dependence on t, then this is the Cartesian product, that is, $S_n = \Omega \times I_n$. The union of all the slabs makes the whole space–time domain $\Omega \times I$.

As mentioned earlier, a global coupling of the variables in the time dimension is not necessary because information is transferred only from earlier to later times. So, one space–time "slab" is solved in each time step, while each "slab" is only one element "high" in the time direction.

Let $\mathcal{E}$ be the 3-dimensional reference spatial element, the vector of basis functions $\mathbf{R}(\xi, \eta, \zeta)$ and its gradients $\nabla\mathbf{R}(\xi, \eta, \zeta)$ will be:

$$\mathbf{R}(\xi, \eta, \zeta) = \left[\varphi_1(\xi, \eta, \zeta), \varphi_2(\xi, \eta, \zeta), \ldots, \varphi_m(\xi, \eta, \zeta)\right] \tag{1}$$

$$\nabla\mathbf{R}(\xi, \eta, \zeta) = \begin{bmatrix} \frac{\partial\varphi_1(\xi,\eta,\zeta)}{\partial\xi} & \frac{\partial\varphi_2(\xi,\eta,\zeta)}{\partial\xi} & \cdots & \frac{\partial\varphi_m(\xi,\eta,\zeta)}{\partial\xi} \\ \frac{\partial\varphi_1(\xi,\eta,\zeta)}{\partial\eta} & \frac{\partial\varphi_2(\xi,\eta,\zeta)}{\partial\eta} & \cdots & \frac{\partial\varphi_m(\xi,\eta,\zeta)}{\partial\eta} \\ \frac{\partial\varphi_1(\xi,\eta,\zeta)}{\partial\zeta} & \frac{\partial\varphi_2(\xi,\eta,\zeta)}{\partial\zeta} & \cdots & \frac{\partial\varphi_m(\xi,\eta,\zeta)}{\partial\zeta} \end{bmatrix} \tag{2}$$

Let $\mathcal{T} = [\tau^1, \tau^3]$ be the *reference* element in time. Assume that the time basis is nodal and linear. In this case, χ^1 and χ^3 are the linear basis functions, while τ^1 and τ^3 are reference nodes. Let $\Delta\tau = |\tau^3 - \tau^1|$ be the length of the time interval in the reference time element, then, the basis functions and their derivatives in the reference time element are:

$$\chi^1(\tau) = \left(\tau^3 - \tau\right)/\Delta\tau \tag{3}$$

$$\chi^3(\tau) = \left(\tau - \tau^1\right)/\Delta\tau \tag{4}$$

$$\frac{d\chi^1(\tau)}{d\tau} = -1/\Delta\tau \tag{5}$$

$$\frac{d\chi^3(\tau)}{d\tau} = 1/\Delta\tau \tag{6}$$

Let $\Re$ be the space–time reference element $\Re = \mathcal{E} \times \mathcal{T}$, then, the basis is:

$$\lambda_{ij}(\xi, \eta, \zeta, \tau) = \varphi_i(\xi, \eta, \zeta)\chi^j(\tau)$$
$$i = 1, \ldots, m;\ j = 1, 3 \tag{7}$$

for $(\xi, \eta, \zeta) \in \mathcal{E}$ and $\tau \in \mathcal{T}$. The space–time node (ξ, η, ζ, τ) ranges over $\Re$.

Now, the space–time nodes in the physical element $\wp$ are given by:

$$\begin{bmatrix} x_1^1 \\ y_1^1 \\ z_1^1 \\ t^1 \end{bmatrix}, \begin{bmatrix} x_2^1 \\ y_2^1 \\ z_2^1 \\ t^1 \end{bmatrix}, \ldots, \begin{bmatrix} x_m^1 \\ y_m^1 \\ z_m^1 \\ t^1 \end{bmatrix}, \begin{bmatrix} x_1^3 \\ y_1^3 \\ z_1^3 \\ t^3 \end{bmatrix}, \begin{bmatrix} x_2^3 \\ y_2^3 \\ z_2^3 \\ t^3 \end{bmatrix}, \ldots, \begin{bmatrix} x_m^3 \\ y_m^3 \\ z_m^3 \\ t^3 \end{bmatrix}$$

where $(x_i^j, y_i^j, z_i^j, t^j) \in \wp$, with $i = 1, \ldots, m$; $j = 1, 3$ is the ith nodal position at time j. The mapping from $\Re$ to the physical element $\wp$ is then given by

$$\begin{bmatrix} x(\xi, \eta, \zeta, \tau) \\ y(\xi, \eta, \zeta, \tau) \\ z(\xi, \eta, \zeta, \tau) \\ t(\tau) \end{bmatrix} = \begin{bmatrix} \sum_{i=1}^m (\lambda_{i1}(\xi, \eta, \zeta, \tau)x_i^1 + \lambda_{i3}(\xi, \eta, \zeta, \tau)x_i^3) \\ \sum_{i=1}^m (\lambda_{i1}(\xi, \eta, \zeta, \tau)y_i^1 + \lambda_{i3}(\xi, \eta, \zeta, \tau)y_i^3) \\ \sum_{i=1}^m (\lambda_{i1}(\xi, \eta, \zeta, \tau)z_i^1 + \lambda_{i3}(\xi, \eta, \zeta, \tau)z_i^3) \\ t^1 + (\Delta t)\frac{(\tau - \tau^1)}{\Delta\tau} \end{bmatrix} \tag{8}$$

where $\lambda_{ij}(\xi, \eta, \zeta, \tau)$ is the basis functions of the space–time element defined in Eq. (7). Δt is the physical time interval length of the current physical interval $[t^1, t^3]$:

$$\Delta t = t^3 - t^1 \tag{9}$$

Now suppose there is a time-dependent velocity field $\mathbf{V}(x, y, z, t)$ defined on the physical domain. Its nodal values on a particular element at time t are given by a $3 \times m$ matrix

$$\mathbf{V}(x, y, z, t) = \begin{bmatrix} v_{1x} & v_{2x} & \dots & v_{mx} \\ v_{1y} & v_{2y} & \dots & v_{my} \\ v_{1z} & v_{2z} & \dots & v_{mz} \end{bmatrix} \tag{10}$$

In this study, the nodal velocities $[v_{ix}, v_{iy}, v_{iz}]^T, i = 1, 2, \dots, m$, are considered to be constant in time on each time interval $[t_n, t_{n+1}]$.

If we consider the spatial nodes in the physical element at any time in interval $[t^1, t^3]$ be advected from time t^1 under the velocity field $\mathbf{V}$, then the space–time nodes can be given by:

$$\begin{bmatrix} x(\xi,\eta,\zeta,\tau) \\ y(\xi,\eta,\zeta,\tau) \\ z(\xi,\eta,\zeta,\tau) \\ t(\tau) \end{bmatrix} = \begin{bmatrix} \sum_{i=1}^m \varphi_i x_i^1 + (\Delta t)\frac{(\tau-\tau^1)}{\Delta\tau} \sum_{i=1}^m \varphi_i v_{ix} \\ \sum_{i=1}^m \varphi_i y_i^1 + (\Delta t)\frac{(\tau-\tau^1)}{\Delta\tau} \sum_{i=1}^m \varphi_i v_{iy} \\ \sum_{i=1}^m \varphi_i z_i^1 + (\Delta t)\frac{(\tau-\tau^1)}{\Delta\tau} \sum_{i=1}^m \varphi_i v_{iz} \\ t^1 + (\Delta t)\frac{(\tau-\tau^1)}{\Delta\tau} \end{bmatrix} \tag{11}$$

where $\varphi_i = \varphi_i(\xi, \eta, \zeta)$, $i = 1, 2, \dots, m$, is the basis function of the space element defined in Eq. (1). This mapping has the characteristic that any points in the reference element with the same time τ will be mapped to the points in the physical element with the same time t. The Jacobian matrix is:

$$\begin{aligned} \mathbf{J}(\xi,\eta,\zeta,\tau) &= \begin{bmatrix} x_\xi & x_\eta & x_\zeta & x_\tau \\ y_\xi & y_\eta & y_\zeta & y_\tau \\ z_\xi & z_\eta & z_\zeta & z_\tau \\ t_\xi & t_\eta & t_\zeta & t_\tau \end{bmatrix} \\ &= \begin{bmatrix} x_\xi & x_\eta & x_\zeta & x_\tau \\ y_\xi & y_\eta & y_\zeta & y_\tau \\ z_\xi & z_\eta & z_\zeta & z_\tau \\ 0 & 0 & 0 & t_\tau \end{bmatrix} \end{aligned} \tag{12}$$

where the subscripts mean partial derivatives. By substituting Eq. (11) to (12), the Jacobian matrix then becomes:

$$\mathbf{J} = \begin{bmatrix} J(\xi,\eta,\zeta) + (\Delta t)\frac{(\tau-\tau^1)}{\Delta\tau}\mathbf{V}\nabla\mathbf{R}(\xi,\eta,\zeta)^{\mathrm{T}} & \frac{\Delta t}{\Delta\tau}\mathbf{V}\mathbf{R}(\xi,\eta,\zeta)^{\mathrm{T}} \\ 0 & \frac{\Delta t}{\Delta\tau} \end{bmatrix} \tag{13}$$

where $J(\xi, \eta, \zeta)$ is the spatial element Jacobian at time t_1,

$$J(\xi,\eta,\zeta) = \begin{bmatrix} \sum_{i=1}^m \frac{\partial\varphi_i}{\partial\xi} x_i^1 & \sum_{i=1}^m \frac{\partial\varphi_i}{\partial\eta} x_i^1 & \sum_{i=1}^m \frac{\partial\varphi_i}{\partial\zeta} x_i^1 \\ \sum_{i=1}^m \frac{\partial\varphi_i}{\partial\xi} y_i^1 & \sum_{i=1}^m \frac{\partial\varphi_i}{\partial\eta} y_i^1 & \sum_{i=1}^m \frac{\partial\varphi_i}{\partial\zeta} y_i^1 \\ \sum_{i=1}^m \frac{\partial\varphi_i}{\partial\xi} z_i^1 & \sum_{i=1}^m \frac{\partial\varphi_i}{\partial\eta} z_i^1 & \sum_{i=1}^m \frac{\partial\varphi_i}{\partial\zeta} z_i^1 \end{bmatrix}$$

and $\nabla\mathbf{R}(\xi, \eta, \zeta)$ is a $3 \times m$ matrix defined in Eq. (2).

3. Convection–diffusion thermal problem

3.1. Governing equations

The general convection–diffusion heat transfer (transport) equation, with divergence free velocity field, will be:

$$\rho c_p\left(\frac{\partial T}{\partial t} + \mathbf{u}\cdot\nabla T\right) - \nabla(k\nabla T) = Q \tag{14}$$

or

$$\frac{\partial T}{\partial t} + \mathbf{u}\cdot\nabla T - \alpha\Delta T = \frac{Q}{\rho c_p} \tag{15}$$

where T is the temperature field, $\mathbf{u}$ is the given convective velocity field, and $\alpha = k/\rho c_p$ is the thermal diffusivity, where ρ and c_p are the mass density and specific heat at constant pressure, respectively. k is the thermal conductivity. Q is a heat source term.

The initial condition can be expressed as:

$$T(x, y, z, 0) = T_0(x, y, z), \quad (x, y, z) \in \Omega \tag{16}$$

where Ω is the physical domain.

The boundary conditions depend on α. In the case of pure convection, $\alpha = 0$, the boundary condition becomes Dirichlet on the inflow boundary:

$$T = T_D, \quad \text{on } \Gamma^{\text{in}} \tag{17}$$

In this paper, we focus on the case in which $\alpha > 0$ and the boundary conditions are:

$$T = T_D \quad \text{on } \Gamma^D \quad \text{(Dirichlet boundary)} \tag{18}$$

$$\alpha\nabla T\cdot\mathbf{n}(x, y, z) = f_x \quad \text{on } \Gamma^N \quad \text{(Neumann boundary)} \tag{19}$$

where $\mathbf{n}(x, y, z)$ is the outward normal at point (x, y, z) on boundary Γ^N.

3.2. Space–time finite element formulation

The temperature field T defined on a space–time slab S_n can be written as $T(x, y, z, t)$, where $(x, y, z) \in \Omega(t)$ and t is in the interval I_n. The solution is defined on each slab S_n. The boundary of $\Omega(t)$ is denoted by $\Gamma(t)$, and is a union of a Dirichlet part $\Gamma^D(t)$ and a Neumann part $\Gamma^N(t)$. In a pure advection problem, with given velocity field $\mathbf{u}$, $\Gamma^N(t)$ is empty, and $\Gamma^D(t)$ consists of the inlet boundary, which is

$$\Gamma^{\text{in}}(t) = \left\{(x, y, z) \in \Gamma(t) \mid \mathbf{u}(x, y, z)\cdot\mathbf{n}(x, y, z) < 0\right\} \tag{20}$$

We use W_n to denote the space–time "slab" corresponding to the chosen discretization on S_n. W denotes the whole space–time domain on which the space of test functions θ is defined, i.e., $\theta \in W$ and $\theta|_{S_n} \in W_n$. As usual, T must satisfy the Dirichlet conditions and θ must satisfy the homogeneous Dirichlet conditions.

By applying the characteristic streamline diffusion (CSD) method [16,17], the space–time FE method may now be formulated as follows: for $n = 0, 1, \dots, \mathbb{N}$, find $T \in W_n$ such that

$$\begin{aligned} &\int_{S_n}\left(\frac{\partial T}{\partial t} + \mathbf{u}\cdot\nabla T\right)\left(\theta + \delta\left[\frac{\partial\theta}{\partial t} + \mathbf{u}\cdot\nabla\theta\right]\right) dx\,dy\,dz\,dt \\ &\quad + \int_{S_n} \alpha'\nabla T\cdot\nabla\theta\,dx\,dy\,dz\,dt \\ &\quad + \int_{\Omega} \left(T_n^+ - T_{n-1}^-\right)\theta_n^+\,dx\,dy\,dz \\ &= \int_{S_n} \frac{Q}{\rho c_p}\left(\theta + \delta\left[\frac{\partial\theta}{\partial t} + \mathbf{u}\cdot\nabla\theta\right]\right) dx\,dy\,dz\,dt \end{aligned} \tag{21}$$

Here

$$\theta_n^{\pm} = \lim_{s\to 0^+} \theta(t_n \pm s) \tag{22}$$

and

$$\delta = \frac{C}{(1+|\mathbf{u}|^2)^{1/2}} \max\left(h - \frac{\alpha}{(1+|\mathbf{u}|^2)^{1/2}}, 0\right) \tag{23}$$

where $C \simeq 1$ and h is a measure of the local mesh size (e.g., the average element diameter). Note that data are transfered from one slab to the next via a built-in L_2-projection in the jump term

$$\int_{\Omega} \left(T_n^+ - T_{n-1}^-\right)\theta_n^+ \, dx\, dy\, dz \tag{24}$$

Furthermore, let r be a measure of the size of the residual on S_n:

$$r = \left(\frac{|T_n{}^+ - T_{n-1}{}^-|}{(t^{n+1}-t^n)} + \left|\frac{\partial T}{\partial t} + \mathbf{u}\cdot\nabla T\right|\right) \Big/ \max_{S_n} |T| \tag{25}$$

where the terms in the numerator represents L^2 norms over Ω and S_n, respectively. Then, by considering the residual, the modified thermal diffusivity is:

$$\alpha' = \max\left(\alpha, Ch^2 r\right) \tag{26}$$

3.3. Domain, initial and boundary conditions

The initial condition for the thermal analysis depends on the welding process: with or without pre-heating, single- or multi-pass, and so on. Normally, for a single-pass weld without pre-heating, the initial temperature field will be set to a constant value equal to the temperature of the surrounding medium.

Three types of boundary conditions occur in the thermal analysis of welding process: (1) Dirichlet BC (isothermal boundary condition), the temperature is prescribed; (2) Neumann or flux BC, the heat flow density is prescribed; (3) Robin or convection BC, the heat transfer to the surrounding medium is proportional to the difference between surface temperature and the surrounding medium temperature.

Fig. 1 shows a scheme of the domain and boundary conditions for the convection–diffusion heat flow analysis in the weld pool or weld joint region. Γ_0 is the inlet surface, normally it is set to be a Dirichlet BC. Γ_1 usually has the flux BC or Dirichlet BC, which represents heat input. Γ_2 is the top surface, which is usually set to a convection BC that includes radiation effects. Γ_3 is the bottom surface that can be a convection BC, a Neumann BC or a Dirichlet BC. Γ_4 are the side surfaces, which can be a Neumann BC, a convection BC or a Dirichlet BC depending on the problem. Γ_5 is the outlet surface on which a flux BC is normally applied.

3.4. Melting and solidification

In the molten pool region, the filler metal and base metal will first melt when heating, then solidify when cooling. Latent heat should be considered in the thermal analysis for the welding process. An enthalpy method is used for melting and solidification. In this case, the enthalpy increment is used to compute the residual. The transient convection–diffusion equation (Eq. (14)) could be written as:

$$\frac{\partial H}{\partial t} + \mathbf{u}\cdot\nabla H - \nabla\cdot(k\nabla T) = Q \tag{27}$$

where H is the enthalpy.

4. Tests and results

4.1. One-dimensional transient conduction problem

Consider a semi-infinite one-dimensional bar with $0 \leqslant x < \infty$. The bar is initially at a constant temperature T_0 throughout, when suddenly (at time $t = 0$) the end at $x = 0$ is changed to T_f, the final temperature, and set as a Dirichlet BC. If its side surfaces have zero Neumann BC (zero flux), then, the transient temperature distribution can be written as:

$$\frac{T - T_f}{T_0 - T_f} = \operatorname{erf}\left(\frac{x}{2\sqrt{\alpha t}}\right) \tag{28}$$

where T is the temperature at point x at time t. This test is designed to test the transient term and diffusion term of the energy equation.

The numerical test was performed on a bar mesh with the size of 1 m × 0.01 m × 0.01 m. To accommodate a sharper temperature gradient, a finer grid was used at the $x = 0$ end (Fig. 2). The material is a low-alloy steel, with the diffusivity $\alpha = 1.13 \times 10^{-5}\ \mathrm{m^2\,s^{-1}}$. The initial temperature $T_0 = 300$ K. The Dirichlet temperature at $x = 0$ m is $T_f = 400$ K.

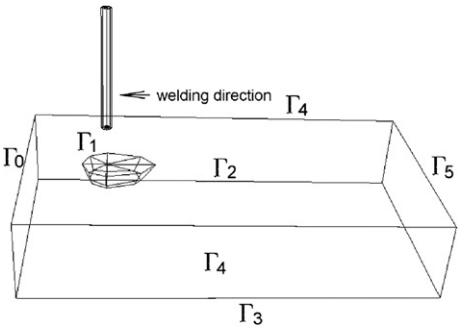

Fig. 1. Domain and boundary conditions for the thermal analysis on the weld pool or the weld joint region.

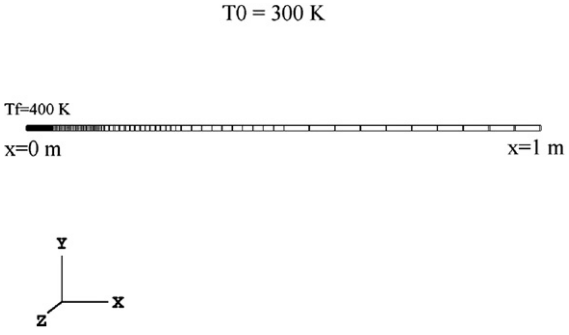

Fig. 2. Bar mesh for the one-dimensional transient conduction problem.

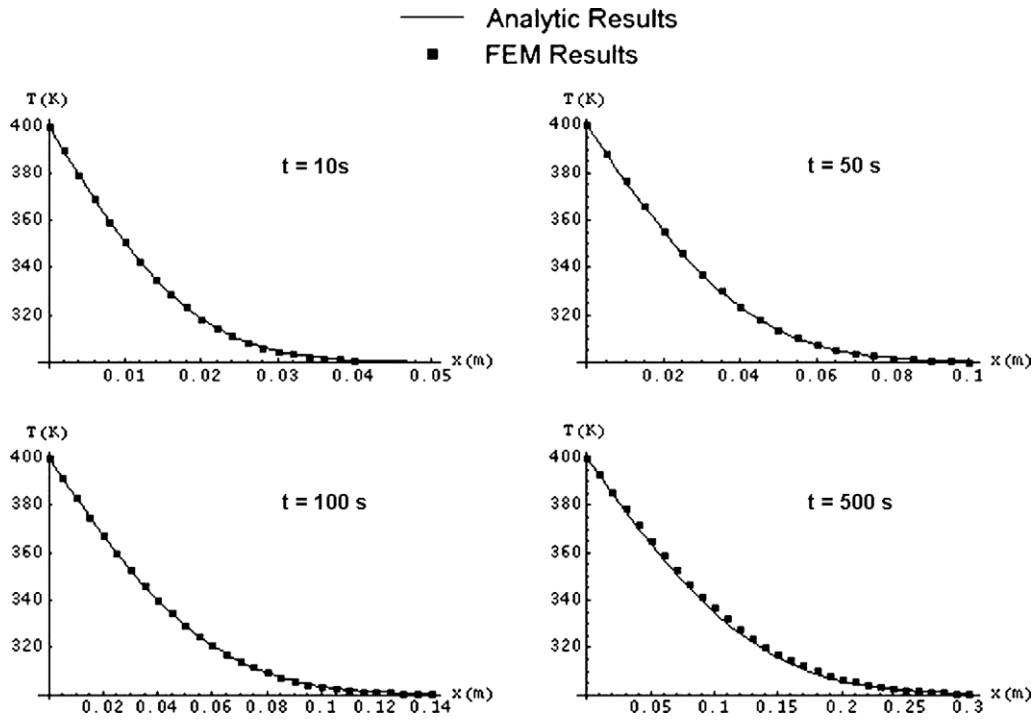

Fig. 3. The analytic and numerical results for one-dimensional transient conduction problem.

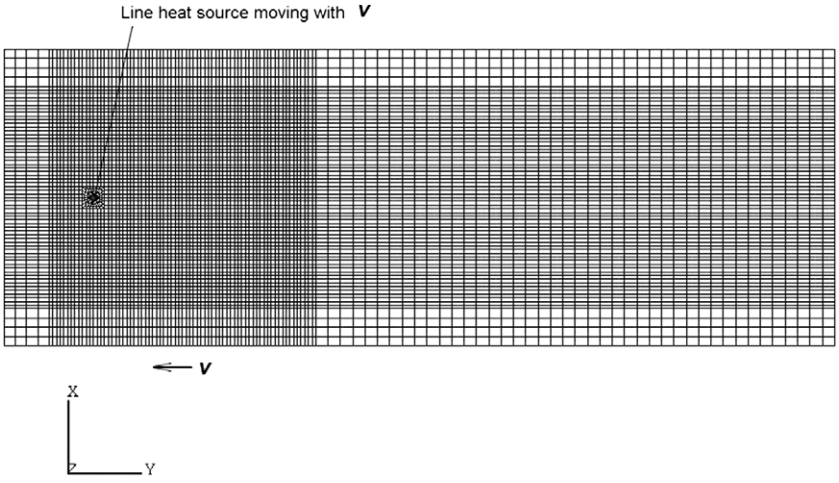

Fig. 4. Mesh for moving line heat source in the infinite plate problem.

Both analytic and numerical results are shown in Fig. 3. It can be seen that the numerical results agree very well with the analytic results.

4.2. Moving line heat source in the infinite plate

The widely used analytic model to simulate a butt weld on a thin plate is the moving line heat source in the infinite thin plate. The line-type heat source moves at a constant speed in the infinitely extended thin plate. Because of the small thickness of the workpiece, temperature variations in the thickness direction are assumed negligible. As such it can be treated as a two-dimensional problem. The analytic solution for a steady state temperature distribution T in the plate was provided by Rykalin [2]:

$$T - T_0 = \frac{q}{2\pi k \Delta} e^{-vx/2\alpha} R_0\left(r\sqrt{\frac{v^2}{4\alpha^2} + \frac{b}{\alpha}}\right) \tag{29}$$

where T_0 is the initial temperature, q is the heat transferred from heat source to plate, Δ is the thickness of the plate, k is the thermal conductivity, v is the velocity of the moving heat source, α is the thermal diffusivity. R_0 is the modified Bessel function of the second kind and zero order. b is a coefficient for heat loss, defined as:

$$b = 2(\lambda_c + \lambda_r)/(\rho c_p \Delta) \tag{30}$$

where λ_c is the coefficient of convective heat transfer, λ_r is the coefficient of heat radiation, ρ is the density, and c_p is the mass-specific heat capacity.

The numerical test was performed on a mesh with the size of $0.24\ \text{m} \times 0.672\ \text{m} \times 0.003\ \text{m}$. The line source is represented by a cylinder with radius $r = 0.0001$ m. A finer grid is used near the heat source to accommodate a steep temperature gradient near the weld pool (Fig. 4). The heat from the line source $q = 3900\ \text{J s}^{-1}$, and the velocity of the moving heat source $v = 0.002\ \text{m s}^{-1}$. The thermal diffusivity $\alpha = 1.13 \times 10^{-5}\ \text{m}^2\,\text{s}^{-1}$ and heat transfer coefficient $b = 0.00377\ \text{s}^{-1}$. The inlet Dirichlet temperature is 300 K.

The FEM thermal result is shown in Fig. 5. To check the validation, a comparison of FEM results with the analytic solution (Eq. (29)) is made (Figs. 6–7). A very good agreement between the numerical results and analytic results is observed.

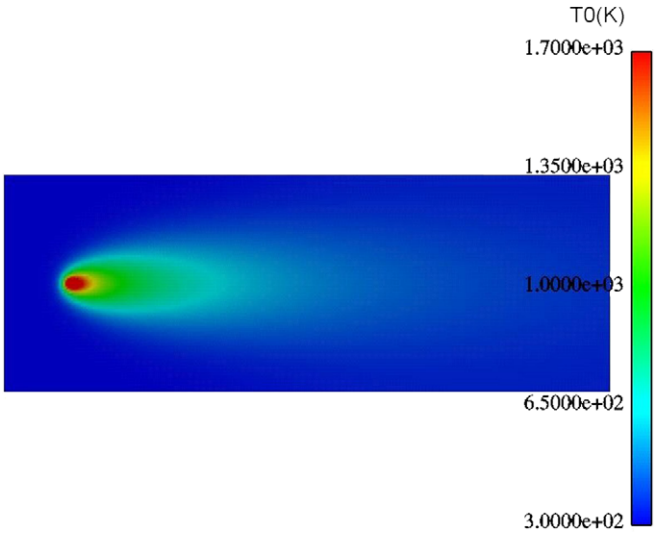

Fig. 5. Temperature field for moving line heat source in the infinite plate problem.

5. Applications

5.1. Thermal analysis on the weld pool of a butt weld

In an arc weld, a highly localized concentrated energy source fuses the filler metal and nearby base metal to form a weld pool. The shape and temperature distribution of a weld pool are dependent on the type of welding processes, welding parameters (welding velocity, diameter of wire, wire feed rate, voltage, current density, angle of workpiece inclination, etc.) and the weld materials. One of the major challenges of computational weld mechanics is to simulate the geometry and temperature distribution of a weld pool accurately and efficiently.

There are several approaches to model the effects of the heat source on a weld pool. One of the simple ways is to prescribe either the thermal flux or power density distribution, or the temperature distribution in the weld pool by a distribution function that intend to model the heat input. Some examples are the double-ellipsoid model provided by Goldak et al. [19] for most realistic welds with simple shapes, and the compound-ellipsoid

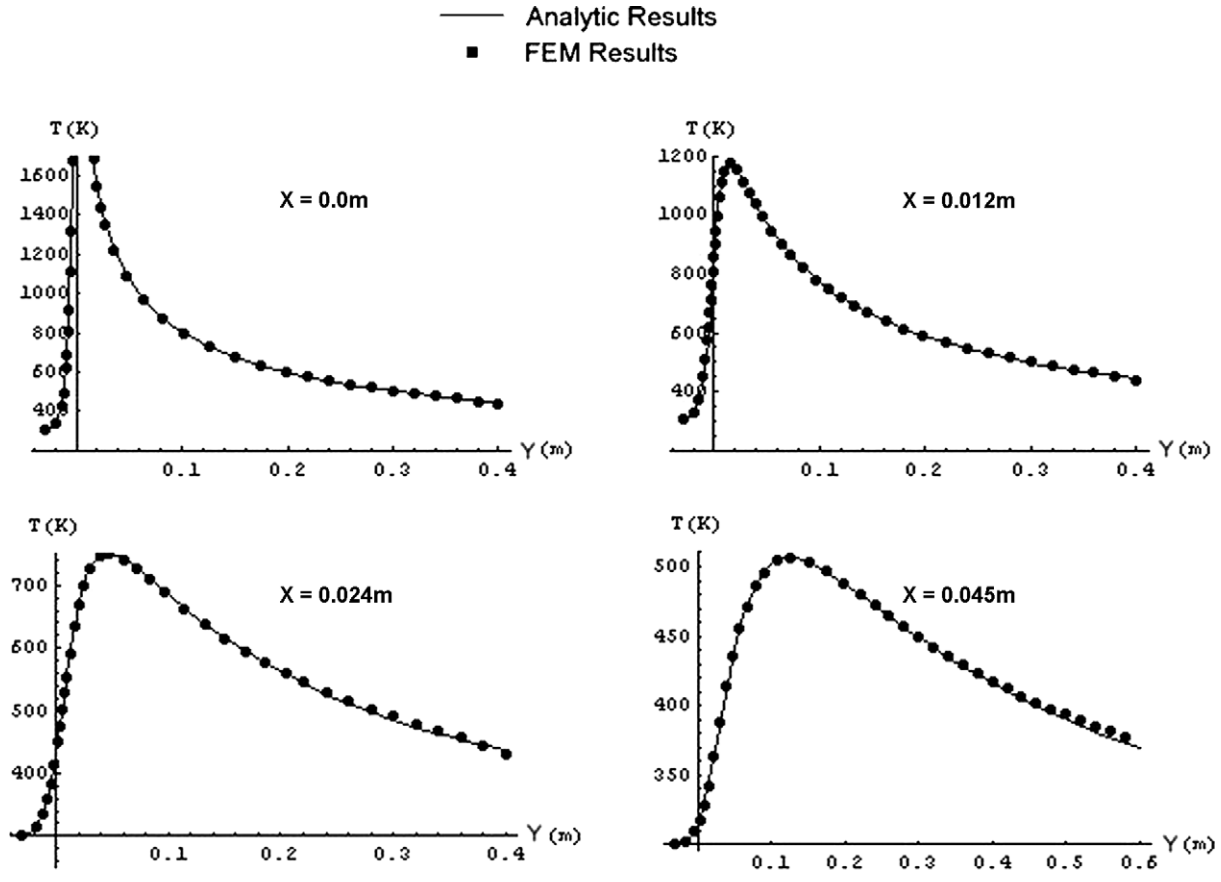

Fig. 6. Longitudinal temperature distribution for moving line heat source in the infinite plate problem.

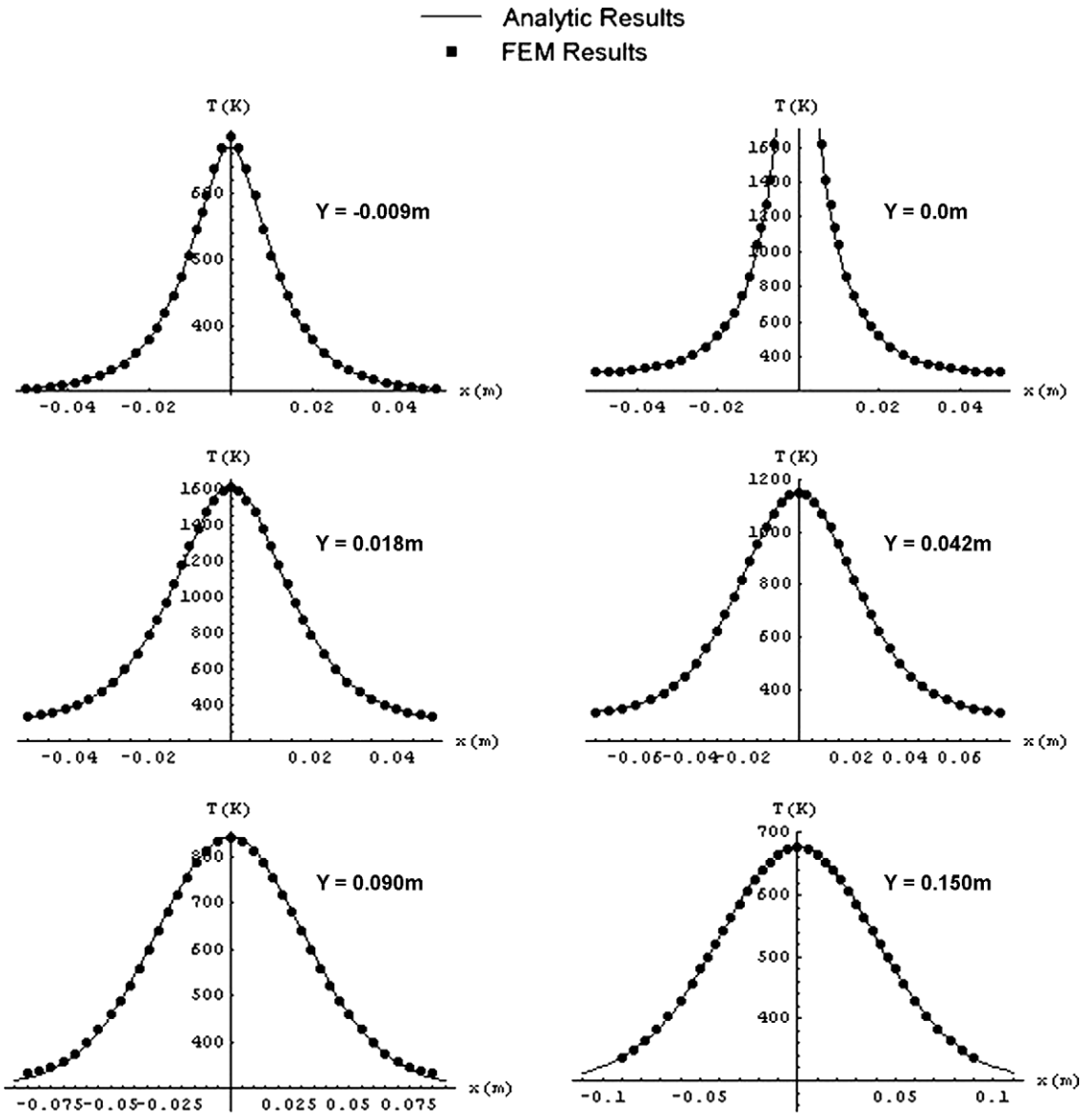

Fig. 7. Transverse temperature distribution for moving line heat source in the infinite plate problem.

model by Gu et al. [20] for a more complicated shape which can occur in high power submerged arc welds. These models are convenient, accurate, efficient and flexible in an application as long as the geometry of the liquid–air surface of the molten pool does not need to be considered.

The energy transport (heat flow) is influenced not only by the content of enthalpy, but also by the deformation of the weld pool, especially the deformation of the molten pool surface profile. For some applications, such as welding a pipe, or a workpiece with very large inclination angle (such as vertical or overhead), the weld pool can be heavily deformed, due to gravity, arc pressure and surface tension. In such cases, the weld pool analysis should consider the geometry of the weld pool surface.

In this section, a model based on the force balance among gravity, arc pressure and surface tension, that predicts both the temperature distribution in the weld pool and the surface geometry of the molten pool, is briefly presented that can deal with many different welding applications.

5.1.1. The hydrostatic surface tension model

The physical phenomena in and around the weld pool during welding are very complicated. The simplification made in this model is based on the following assumptions:

- The influence of the fluid flow in the molten pool on the heat flow could be neglected;
- The weld pool is considered to be in a quasi-steady state;
- The heat flow density (flux) transferred from the welding arc to the weld pool is assumed to follow a model provided by Weiss [21] which depends on the electrical resistance in the plasma of the arc. The corresponding distribution function is:

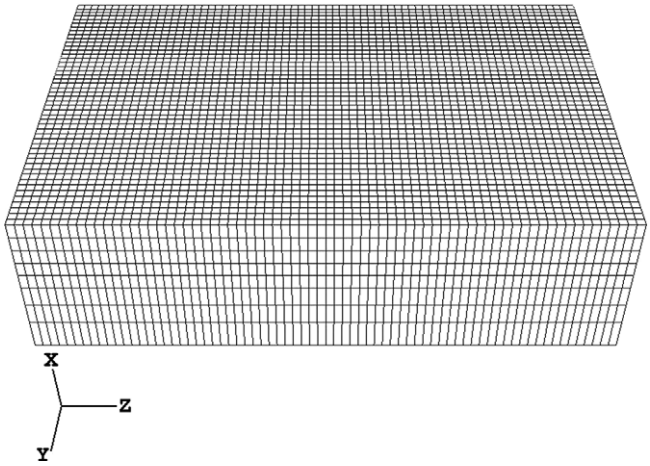

Fig. 8. Mesh for weld pool problem.

$$\Phi(x, y, z, T) = \exp\left(-\frac{R^2 - R_{\min}^2}{R_{\max}^2 - R_{\min}^2}\right) \tag{31}$$

where R is the electrical resistance on a line from the electrode tip to a point on the weld pool surface with temperature (x, y, z, T);

- The pool surface is assumed to be in a static equilibrium with respect to gravity, arc pressure and surface tension. The influence of buoyancy, inertial force and the electromagnetic force are disregarded. So, for each point on the surface, a static force balance in the normal direction is assumed over the surface among arc pressure, surface tension and hydrostatic pressure [21,22].

5.1.2. Results

The weld pool model was tested on a flat weld pool mesh (Fig. 8) to simulate the formation of the weld pool surface and the temperature distribution on the upper side of a horizontal workpiece. The thermal results of the weld pool will be used as a heat source for the thermal analysis of a weld joint (see Section 5.2).

A weld pool domain of size 0.01 m × 0.024 m × 0.038 m was a sub-domain cut from a butt weld thermal problem with size of 0.01 m × 0.12 m × 0.25 m. The material was a low alloy steel. The heat input $Q = 1900\ \mathrm{J\,s^{-1}}$, and welding velocity $v = 0.002\ \mathrm{m\,s^{-1}}$. The inlet surface was set to be a Dirichlet boundary condition, with Dirichlet temperature $T_D = 300$ K. The outlet surface was set to be a flux boundary condition. The flux data was from the thermal results of the larger domain by domain decomposition. The upper and bottom surfaces are natural convection boundary conditions. The side surfaces are Dirichlet boundary conditions, with the temperature values from the thermal results of the larger domain by domain decomposition. The molten zone shape and temperature distribution were shown in Figs. 9 and 10.

5.2. Thermal analysis on a butt weld joint

A thermal analysis of a butt weld joint was also presented here as one application. It was performed on a mesh 0.01 m thick, 0.12 m wide and 0.25 m long (Fig. 11). The coordinates are x: the thickness direction; y: the lateral direction; and z: the longitudinal direction. The moving mesh was fixed with the heat source with the welding speed at 0.002 $\mathrm{m\,s^{-1}}$ in z-direction. The center of the weld pool was 0.025 m from the leading edge. The material was low-alloy steel with temperature-dependent properties.

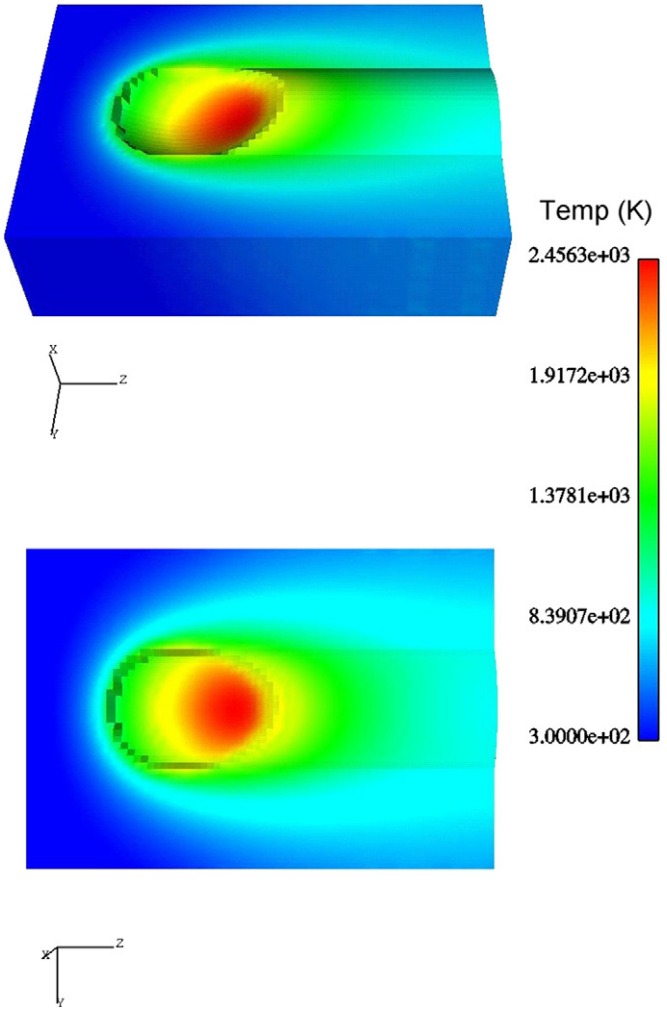

Fig. 9. Weld pool thermal result of a butt weld.

The inlet surface was a Dirichlet boundary condition, with the Dirichlet temperature $T_D = 300$ K. The outlet surface was a zero flux boundary condition. The other four surfaces were a natural convection boundary condition. The heat source was provided by the hydrostatic surface tension weld pool model discussed in Section 5.1.

The temperature field from the weld pool analysis (Figs. 9 and 10) was used as a Dirichlet temperature in the weld pool region. In detail, the temperature field from the weld pool model was mapped to the current weld joint domain, all the nodes with temperature greater than 1200 K were set to the Dirichlet temperature. After 30 time steps, with each time step size 4 seconds, the temperature field reached a quasi-stationary state. The steady state results of this test (Figs. 12–13) will be used to analyze microstructure evolution and stresses.

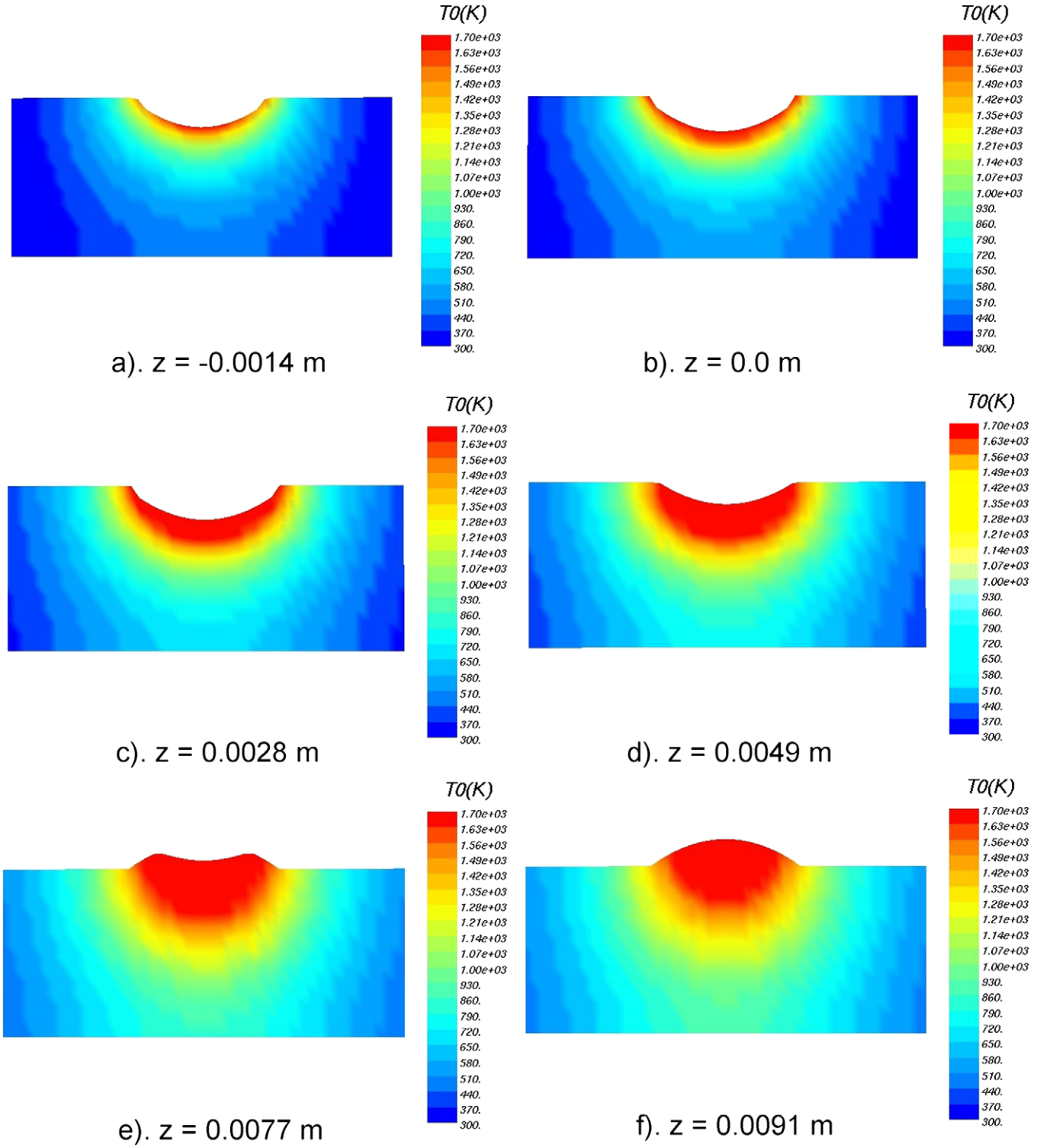

Fig. 10. Weld pool cross section of a butt weld.

6. Conclusions

A space–time finite element method (FEM) has been used to analyze the transient thermal cycle during the welding process by solving the convection–diffusion thermal equation. The Eulerian formulation can provide higher spatial resolution compared to the usual Lagrangian formulation. The model can also include the addition of the filler metal during thermal analysis. The model was tested with problems that have analytic solutions. The numerical results fit the analytic results very well. The thermal tests show that the space–time FE method is appropriate to deal with the 3D thermal analysis in the weld pool and/or weld joint domain which is fixed with the heat source. It can provide both the transient and

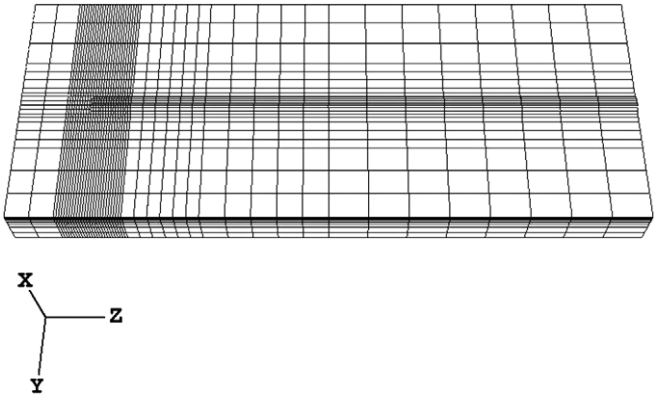

Fig. 11. Mesh for a butt weld thermal analysis.

quasi-stationary results. The thermal cycle of a material point can be obtained by traversing geometry space along a flow line and mapping data into the time dimension. The thermal results obtained can be used to analyze the microstructure evolution in the fusion zone (FZ) and heat affected zone (HAZ).

Acknowledgements

The authors would like to thank the National Science and Engineering Research Council of Canada (NSERC) and the Material Manufacturing Ontario (MMO) for the financial support.

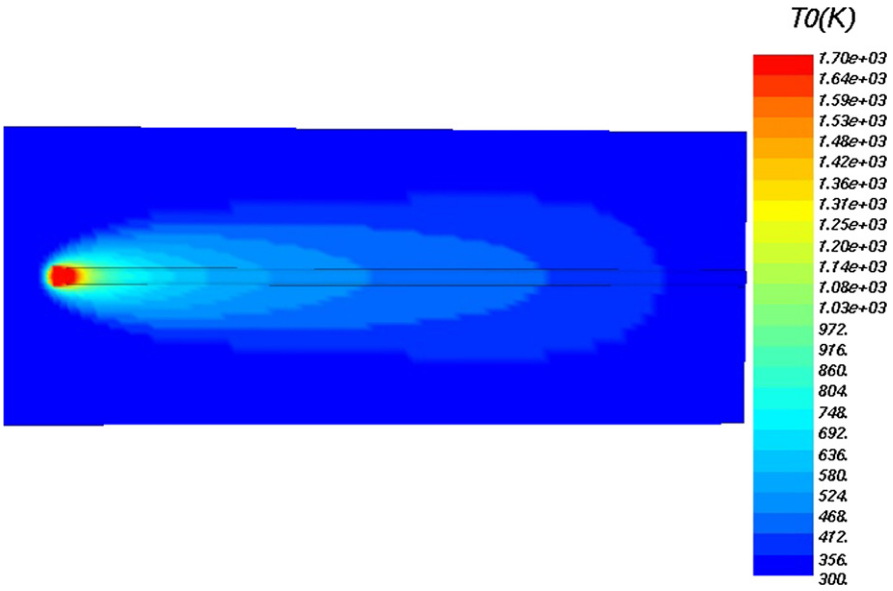

Fig. 12. Top view of temperature distribution for a butt weld thermal analysis.

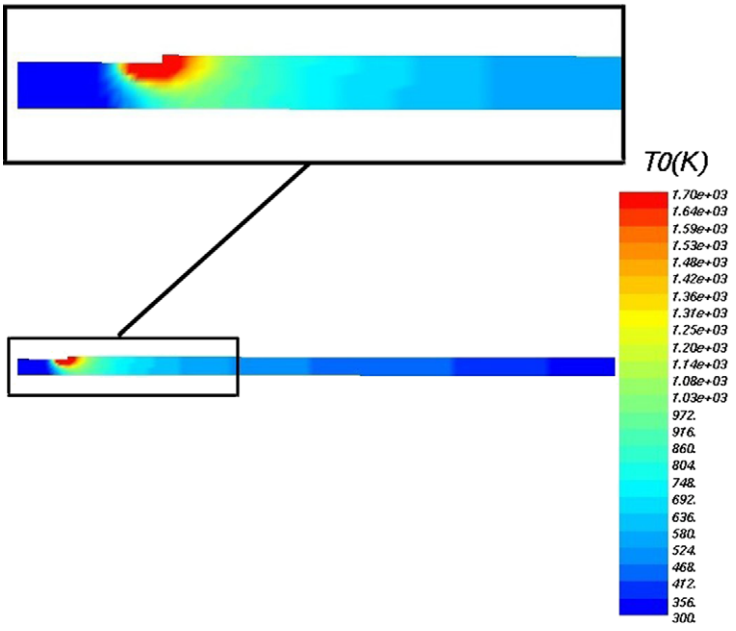

Fig. 13. Temperature distribution at the mid-plane for a butt weld thermal analysis.

References

[1] D. Rosenthal, The theory of moving sources of heat and its application to metal treatment, Trans. ASME 68 (1946) 849–865.

[2] R.R. Rykalin, Calculation of Heat Processes in Welding, Educational Lecture, Am. Weld. Soc. Annual Assembly, New York, 1961.

[3] D. Radaj, Heat Effects of Welding, Springer-Verlag, 1992.

[4] Y. Ueda, H. Murakawa, Applications of computer and numerical analysis techniques in welding research, Trans. JWRI 13 (1984) 337–346.

[5] J.H. Argyris, J. Szimmat, K.J. Willam, Computational aspects of welding stress analysis, Comp. Meth. Appl. Mech. Eng. 33 (1982) 635–666.

[6] J.A. Goldak, Modeling thermal stresses and distortions in welds, in: Recent trends in welding science and technology, in: TWR'89, Proc. of the 2nd International Conference on Trends in Welding Research, Gatlinburg, Tennessee, USA, 14–18 May, 1989.

[7] M. Gu, J.A. Goldak, E. Hughes, Steady state thermal analysis of welds with filler metal addition, Can. Metall. Q. 32 (1993) 49–55.

[8] J.M. McDill, J.A. Goldak, A.S. Oddy, M.J. Bibby, Isoparametric quadrilaterals and hexahedrons for mesh-grading algorithms, Comm. Appl. Num. Meth. 3 (1986) 155–163.

[9] J. Goldak, A. Oddy, M. Gu, W. Ma, A. Mashaie, E. Hughes, Coupling heat transfer, microstructure evolution and thermal stress analysis in weld mechanics, IUTAM Symposium, Lulea, Sweden, June 10–14, 1991.

[10] S.M. Rajadhyaksha, P. Michaleris, Optimization of thermal processes using an Eulerian formulation and application in laser surface hardening, Int. J. Num. Methods Eng. 47 (2000) 1807–1823.

[11] X. Chen, M. Becker, L. Meekisho, Welding analysis in moving coordinates, in: H. Cerjak (Ed.), Mathematical Modelling of Weld Phenomena, vol. 4, Institute of Materials, UK, 1998, pp. 396–410.

[12] E.P. DeGarmo, J.L. Meriam, F. Jonassen, The effect of weld length upon the residual stresses of unrestrained butt welds, Welding Research (Suppl.) (1946) 485–487.

[13] C. Johnson, Finite element methods for convection–diffusion problems, in: R. Glowinski, J.L. Lions (Eds.), Computing Methods in Engineering and Applied Sciences, vol. V, North-Holland, 1982, pp. 311–323.

[14] T.J.R. Hughes, G.M. Hulbert, Space–time element methods for elastodynamics: Formulations and error estimates, Comp. Meth. Appl. Mech. Eng. 66 (1988) 339–363.

[15] F. Shakib, T.J.R. Hughes, A new finite element formulation for computational fluid dynamics: IX. Fourier analysis of space–time Galerkin/least-squares algorithms, Comp. Meth. Appl. Mech. Eng. 87 (1991) 35–58.

[16] P. Hansbo, The characteristic streamline diffusion method for convection–diffusion problems, Comp. Meth. Appl. Mech. Eng. 96 (1992) 239–253.

[17] K. Eriksson, C. Johnson, Adaptive streamline diffusion finite element methods for stationary convection–diffusion problems, Math. Comp. 60 (1993) 167–188.

[18] O.C. Zienkiewics, R.L. Taylor, J.Z. Zhu, The Finite Element Method: Its Basis and Fundamentals, sixth ed., Elsevier–Butterworth–Heinemann, 2005.

[19] J.A. Goldak, A. Chakravarti, M.J. Bibby, A new finite element model for welding heat sources, Metallurgical Trans. AIME 15B (1984) 299–305.

[20] M. Gu, J.A. Goldak, M.J. Bibby, Computational heat transfer in welds with complex weld pool shapes, Advanced Manufacturing Engineering 3 (1991) 31–36.

[21] D. Weiss, U. Franz, J. Schmidt, A model of temperature distribution and weld pool deformation during arc welding, in: H. Cerjak (Ed.), Mathematical Modelling of Weld Phenomena, The Institute of Materials, 1995, pp. 22–39.

[22] T. Ohji, K. Nishiguchi, Mathematical modelling of a molten pool in arc welding of thin plate, Technology Reports of the Osaka Univ. 33 (1983) 35–43.